

# Search for WIMP Inelastic Scattering Off Xenon Nuclei With Xenon100 Data

(The XENON100 Collaboration)

(Dated: January 16, 2017)

Some nice abstract here.....

## I. INTRODUCTION

Astrophysical and cosmological evidence indicates that the dominant mass fraction of our Universe consists of some yet unknown form of dark, or invisible matter. The dark matter could be made of new, yet undiscovered particles, and well-motivated theoretical models going beyond the Standard Model of particle physics predict the existence of Weakly Interacting Massive Particles (WIMPs), which are natural candidates for dark matter. This hypothesis is currently being tested by several direct and indirect detection experiments, as well as at the LHC [1, 2].

Most direct detection searches focus on elastic scattering of galactic dark matter particles off nuclei, where the keV-scale nuclear recoil energy is to be detected [3–5]. In this work, the alternative process of inelastic scattering is explored, where a WIMP-nucleus scattering induces a transition to a low-lying excited nuclear state. The experimental signature is a nuclear recoil detected together with the prompt de-excitation photon [6].

We consider the  $^{129}\text{Xe}$  isotope, which has an abundance of 26.4% in natural xenon, and a lowest-lying  $3/2^+$  state at 36.6 keV above the  $1/2^+$  ground state. The electromagnetic nuclear decay has a half-life of 0.97 s. The signatures of inelastic scattering in xenon have been studied in detail in [7]. It was found that this channel is complementary to spin-dependent, elastic scattering, dominating the integrated rates above  $\simeq 10$  keV energy deposits. In addition, in case of a positive signal, the observation of inelastic scattering would provide a clear indication of the spin-dependent nature of the fundamental interaction.

Our paper is structured as follows. In Section II we briefly describe the XENON100 detector and the employed data set in this analysis. In Section III we detail the data analysis method, including the simulation of the expected signal and the background model. We conclude in Section IV with our results and new constraints on inelastic WIMP-nucleus scatters.

## II. THE XENON100 DETECTOR

The XENON100 experiment operated a dual-phase (liquid and gas) xenon time projection chamber (TPC) at the Laboratori Nazionali del Gran Sasso (LNGS) in Italy. It contained 161 kg of xenon in total, with 62 kg in the active region of the TPC. These were monitored by 242 1-inch square, low-radioactivity, UV-sensitive photomultiplier tubes (PMTs) arranged in two arrays, one in the liquid and one in the gas. The PMTs detected

the prompt scintillation (S1) and the delayed, proportional scintillation signal (S2) created by a particle interacting in the active TPC region. The S2-signal was generated due to ionisation electrons, drifted in a field of 530 V/cm and extracted into the gas phase by a field of 12 kV/cm, where the proportional scintillation, or electroluminescence, was produced. These photons carried the  $x - y$  information of the interaction site, while the  $z$ -information came from the drift time measurement. The TPC thus yielded a three-dimensional event localisation, enabling to reject the majority of background events via fiducial volume cuts, as well as multiple interactions, which are unlikely due to dark matter particles [8]. The ratio of S2/S1 provided the basis for distinguishing between nuclear recoils (NRs), as induced by fast neutrons and expected from elastic WIMP-nucleus scatters, and electronic recoils (ERs) produced by  $\beta$  and  $\gamma$ -rays. As we shall see, the inelastic scattering signature will be a superposition of an ER and a NR, due to the low lifetime of the excited state and the short mean free path ( $\sim 0.15$  mm) of the 39.6 keV photon.

XENON100 has acquired science data between 2008–2015, and has set competitive constraints on spin-independent [9, 10] and spin-dependent [10, 11] elastic WIMP-nucleus scatters, as well as on axions/ALPs [12] and leptophilic dark matter models [13–15].

Here

## III. DATA ANALYSIS

This analysis is performed using XENON100 Run-II science data, which corresponds to an exposure of 224.6 live days. The detector response to electronic recoil (ER) has been characterized using  $^{60}\text{Co}$  and  $^{232}\text{Th}$  radioactive sources, while response to inelastic nuclear recoil (NR) scattering was calibrated using an  $^{241}\text{AmBe}$  source.

The inelastic scattering of a WIMP with the nucleus of  $^{129}\text{Xe}$  produces an energy deposit via nuclear recoil with subsequent emission of a 39.6 keV de-excitation photon. The largest fraction of the energy released in the event is via electronic recoil due to the emitted photon, this represents an unusual signature for this kind of detector and brings the possible signal to overlay a phase space region with large backgrounds. The chosen region of interest (ROI) for this analysis surrounds the 39.6 keV xenon line in the cS1-cS2 plane and is further divided into sub-regions, as shown in Figure 1 and 2.

Events are asked, other than falling in the defined region of interest, to fulfill several selection criteria which can be summarized as: selection aimed to reduce noise

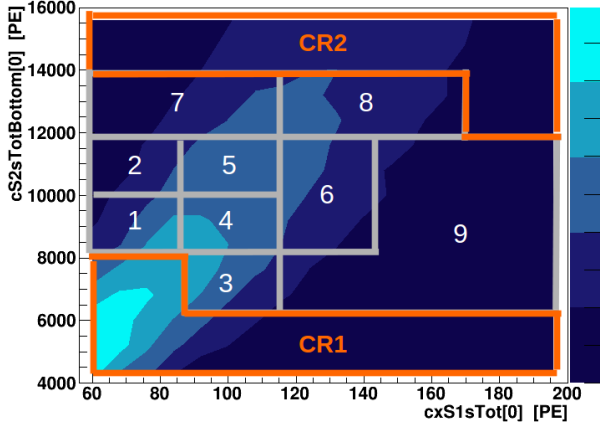


FIG. 1. Signal region and control region.

101 impact and including energy (S1) and S2 thresholds, veto  
 102 of events with energy release in the detector's outer vol-  
 103 ume, and additionally, events must be of single scatter  
 104 nature and fall into a predefined fiducial volume. This  
 105 analysis follows the selection criteria described in detail  
 106 in [?] for Run-II, with only few exceptions reported in  
 107 what follows. The selection on S2 width as a function  
 108 of drift time has been optimized on a sample of events  
 109 selected from the 39.6 keV line and set to a 95% accep-  
 110 tance on these. Events are required to be single scatter  
 111 by applying a threshold on the second largest S2 peak  
 112 size, for this analysis this threshold has been optimized  
 113 to 160 PE and set constant as function of S2 signal size.  
 114 Finally the chosen fiducial volume corresponds to 34 Kg  
 115 of liquid xenon.

### A. Signal Simulation

117 The detector response to inelastic scattering of WIMPs  
 118 off  $^{129}\text{Xe}$  nucleus was simulated using an empirical model.  
 119 The total deposited energy is divided into two inde-  
 120 pendent contributions: one related to the 39.6 keV de-  
 121 excitation photon and the other relative to the simulta-  
 122 neous nuclear recoil of the xenon atom. The number of  
 123 photons and charge yield detected is simulated separately  
 124 for each contribution and then added together.

The distribution in the cS1-cS2 plane of an ER induced  
 by the de-excitation photon is simulated assuming a two  
 dimensional normal pdf,  $f(cS1, cS2)$ , described except a  
 normalization factor in equation 1:

$$f(cS1, cS2) = \exp\left(-\frac{1}{2(1-\rho^2)}\left[\frac{(cS1 - \mu_{cS1})^2}{\sigma_{cS1}^2} + \frac{(cS2 - \mu_{cS2})^2}{\sigma_{cS2}^2} - \frac{2\rho(cS1 - \mu_{cS1})(cS2 - \mu_{cS2})}{\sigma_{cS1}\sigma_{cS2}}\right]\right) \quad (1)$$

125 where  $\mu_{cS1}$  and  $\mu_{cS2}$  represents the average observed cS1  
 126 and cS2 given a 39.6 keVee,  $\sigma_{cS1}$  and  $\sigma_{cS2}$  are the stan-

127 dard deviation in cS1 and cS2 respectively, while  $\rho$  stands  
 128 for the correlation between cS1 and cS2. The detector re-  
 129 lated light yield  $L_y$  at 39.6 keV, necessary to evaluate the  
 130 average number of photon detected ( $\mu_{cS1}$ ), is obtained as  
 131 the result of a NEST model [16–18] fit to data collected  
 132 with several lines. The same model is used to predict the  
 133 charge yield at 39.6 keV which is then scaled according to  
 134 the detector's secondary scintillation gain  $Y$ , determined  
 135 from detector response to single electrons [19]. The de-  
 136 tector resolution at 39.6 keV in cS1 and cS2 has been  
 137 measured to be respectively 15.8% and 14.7% and used  
 138 to extract the standard deviations  $\sigma_{cS1}$ ,  $\sigma_{cS2}$ . The cor-  
 139 relation parameter is assumed to be independent of energy  
 140 (at least in the considered range) and measured using  
 141 the 164 keV xenon activated line by  $^{124}\text{AmBe}$  calibration  
 142 data, this line is chosen since allows to disentangle effi-  
 143 ciently contribution from nuclear recoil. The measured  
 144 correlation is  $\rho = -0.45 \pm 0.10$ .

145 The cS1 and cS2 distributions from NR contribution  
 146 are predicted starting from the nuclear recoil energy spec-  
 147 trum of WIMPs inelastic interaction [?]. The average  
 148 cS1 and cS2 are given by equations 2 and 3 respectively,  
 149 where  $\mathcal{L}_{eff}$  is the liquid xenon NR relative scintillation  
 150 efficiency, while  $S_{ee} = 0.58$  and  $S_{nr} = 0.95$  describe the  
 151 scintillation quenching due to the electric field [20]. The  
 152 parameterization and uncertainties of  $\mathcal{L}_{eff}$  as a function  
 153 of  $E_{nr}$  are based on existing direct measurements [21].  
 154 The light yield at 122 keVee originate from the same  
 155 NEST model fit as described above. For the cS2 the  
 156 parameterization of  $Q_Y(E_{nr})$  is taken from [22]. Finally  
 157 all detector related resolution effects are introduced fol-  
 158 lowing the prescriptions described in [?].

$$cS1_{nr} = E_{nr} \mathcal{L}_{eff}(E_{nr}) L_y \frac{S_{nr}}{S_{ee}} \quad (2)$$

$$cS2_{nr} = E_{nr} Q_Y(E_{nr}) Y \quad (3)$$

159 The pdf of the ER and NR contributions are then con-  
 160 voluted together to obtain the overall pdf of the signal. A  
 161 2D (cS1 versus cS2) acceptance map is applied to the sig-  
 162 nal pdf to reproduce data selection effects. Acceptances  
 163 are computed separately for each selection criteria us-  
 164 ing  $^{124}\text{AmBe}$  calibration sample, selections as the outer  
 165 volume veto and the single scatter interaction represent  
 166 an exception and a dedicated computation has been per-  
 167 formed in these cases. The selections acceptance average  
 168 in the region of interest to about  $0.80 \pm 0.05$ . Figure 1  
 169 shows an example of full simulated signal model for a  
 170 WIMP of 100 GeV mass.

171 The signal simulation procedure has been validated re-  
 172 producing the 39.6 keV xenon line from interaction due  
 173 to  $^{124}\text{AmBe}$  source and has been compared to data. For  
 174 this comparison the proper  $^{124}\text{AmBe}$  nuclear recoil and  
 175 acceptances were simulated. The simulated events were  
 176 found in agreement with calibration data within statisti-  
 177 cal uncertainties.

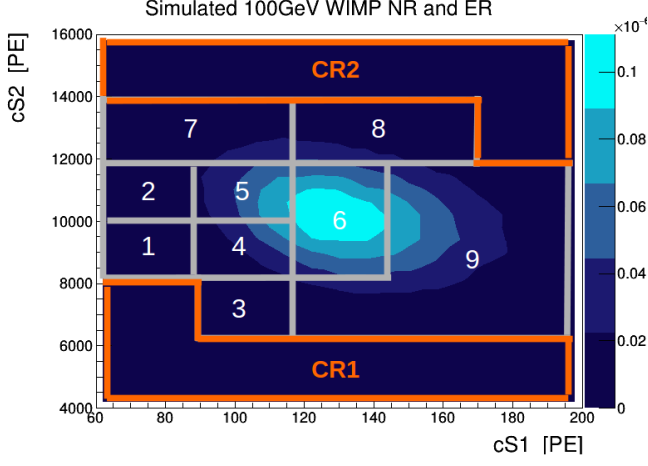


FIG. 2. Signal region and control region, for WIMP of mass 100 GeV.

### B. Background Model

The main expected background contribution in the region of interest is due to environmental and material radioactivity, its composition is mainly represented by Compton scattering photons. Background contribution due to the activation of the xenon 39.6 keV line from radiogenic neutrons is expected to be negligible.

The background is modeled using data from the  $^{60}\text{Co}$  calibration campaign, which are assumed to well represent the background density distribution in the cS1-cS2 plane. The calibration sample yields about 22'000 events in the ROI, these are then scaled to data according to a measured scale factor  $\tau_{bkg}$ . This scale factor, which is merely the ratio between the data and calibration sample yields, is measured in the two control regions shown in Figure 1 and labelled CR1 and CR2. The two control regions give compatible results and the computed average is  $\tau_{bkg} = 0.034 \pm 0.002$ , where the reported uncertainty is of statistical nature only.

The distribution of the calibration sample has been compared to the data of the science run in the two control regions, agreement is found within statistical uncertainties. Furthermore,  $^{60}\text{Co}$  calibration data have been compared in the region of interest to data from  $^{232}\text{Th}$  calibration campaign, the largest deviation between the two shapes is within 4%. An additional systematic uncertainty of 4% has been applied to the expected background yield of each sub-region of the ROI.

### C. Systematic Uncertainties

Uncertainties on the total prediction of background events arise from the uncertainty on the measure of the normalization factor,  $\tau_{bkg}$ , and amount to 6%, contribution of radiogenic neutrons are neglected. Systematic uncertainty on the shape of the predicted background dis-

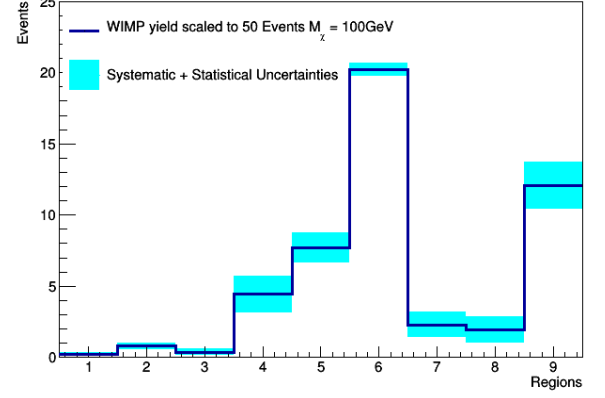


FIG. 3. Signal region, uncertainties for WIMP of mass 100 GeV.

tribution are assessed by the maximal discrepancy in the ROI between the  $^{60}\text{Co}$  and  $^{232}\text{Th}$  calibration samples, a 4% systematic additional to statistical uncertainty is assigned to the expected yield of each sub-region. Note that uncertainties belonging to different sub-regions are considered independent from each other.

Uncertainty on the total yield of signal arising from selections acceptance uncertainties are found to be very weakly dependent on the WIMP mass, an overall 6% acceptance uncertainty is then applied to all WIMPs hypothesis.

Uncertainties on the energy scale and, more generally, related to detector response are parameterized using the respective uncertainties on the measure of  $L_y$ ,  $\mathcal{L}_{eff}$ ,  $Y$ ,  $Q_Y$  and  $\rho$ . The simulation shows that these type of uncertainties mainly affect the pdf of the signal model in the ROI, and very weakly the total signal yield. They are taken into account by simulating several signal pseudo-sample for each WIMP mass, the pseudo-samples are produced varying the model parameters respectively of  $\pm 1$  standard deviation. For each sub-region is then computed an overall uncertainty by adding in quadrature the variations of each pseudo-sample with respect to nominal. Figure 3 is an example of such a systematic uncertainty computation for a WIMP of 100 GeV mass.

All the uncertainties discussed here are parameterized within a binned profiled likelihood function using the framework [23, 24]. All parameters related to systematic uncertainties are assumed to be normally distributed.

## IV. RESULTS

Using an exposure of 34 kg of liquid xenon and 224.6 live days of data a yield of 764 events is observed in the region of interest, this is compatible with the expectation of  $756 \pm 5^{(stat.)} \pm 55^{(syst.)}$  events from the background only hypothesis. Figure 4 shows how these events are distributed in the region of interest, the bottom panel

shows the ratio between data and expected background, where the gray and orange shaded areas represent respectively statistical and systematic uncertainty on the background expectation.

This result is interpreted via a binned profiled likelihood approach by means of the test statistic  $\tilde{q}$  and its asymptotic distributions described in [25]. Assuming an isothermal WIMP halo with a local density of  $\rho_\chi = 0.3 \text{ GeV}/\text{cm}^3$ , a local circular velocity of  $v_0 = 220 \text{ km/s}$ , and a galactic escape velocity of  $v_{esc} = 544 \text{ km/s}$ , other assumptions..., a 90%  $\text{CL}_s$  [26] confidence level limit is computed on the spin dependent inelastic WIMP-nucleon cross section,  $\sigma_{inel}$ , as a function of the WIMP mass,  $m_\chi$ , and shown in Figure 5. The expected median sensitivity is reported with its relative one (green area) and two (yellow area) standard deviation uncertainty. A limit is set on  $\sigma_{inel}$  to  $3.3 \times 10^{-38} \text{ cm}^2$  at 90%  $\text{CL}_s$  confidence level for a WIMP of mass 100 GeV. This limit is compared with decide which other experiment to plot.

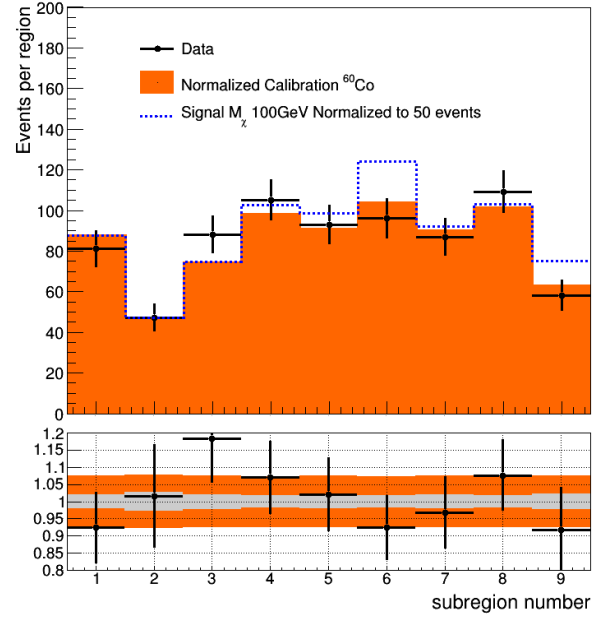


FIG. 4. Results, comparison between data and expected background.

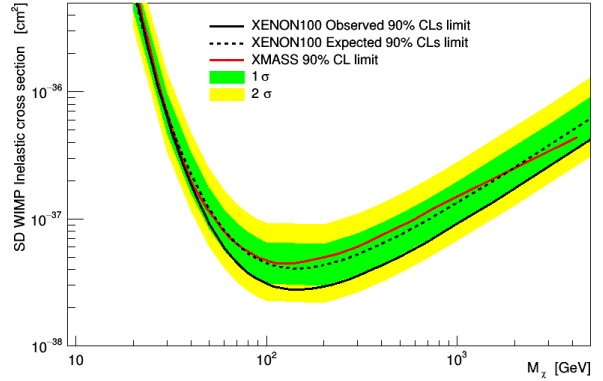


FIG. 5. Observed and expected limits.

- 
- [1] J. Silk et al. *Particle Dark Matter: Observations, Models and Searches*. 2010.
- [2] Laura Baudis. Dark matter detection. *J. Phys.*, G43(4):044001, 2016.
- [3] Laura Baudis. Direct dark matter detection: the next decade. *Phys. Dark Univ.*, 1:94, 2012.
- [4] Laura Baudis. Dark matter searches. *Annalen Phys.*, 528:74, 2016.
- [5] Teresa Marrodn Undagoitia and Ludwig Rauch. Dark matter direct-detection experiments. *J. Phys.*, G43(1):013001, 2016.
- [6] John R. Ellis, R. A. Flores, and J. D. Lewin. Rates for Inelastic Nuclear Excitation by Dark Matter Particles. *Phys. Lett.*, B212:375–380, 1988.
- [7] L. Baudis, G. Kessler, P. Klos, R. F. Lang, J. Menendez, S. Reichard, and A. Schwenk. Signatures of Dark Matter Scattering Inelastically Off Nuclei. *Phys. Rev.*, D88(11):115014, 2013.
- [8] et al Aprile E. The XENON100 Dark Matter Experiment. *Astropart. Phys.*, 35:573–590, 2012.
- [9] E. Aprile et al. Dark Matter Results from 225 Live Days of XENON100 Data. *Phys. Rev. Lett.*, 109:181301, 2012.
- [10] E. Aprile et al. XENON100 Dark Matter Results from a Combination of 477 Live Days. *Phys. Rev.*, D94(12):122001, 2016.
- [11] E. Aprile et al. Limits on spin-dependent WIMP-nucleon cross sections from 225 live days of XENON100 data. *Phys. Rev. Lett.*, 111(2):021301, 2013.
- [12] E. Aprile et al. First Axion Results from the XENON100 Experiment. *Phys. Rev.*, D90:062009, 2014.
- [13] E. Aprile et al. Exclusion of Leptophilic Dark Matter Models using XENON100 Electronic Recoil Data. *Science*, 349(6250):851–854, 2015.
- [14] E. Aprile et al. Search for Event Rate Modulation in XENON100 Electronic Recoil Data. *Phys. Rev. Lett.*, 115(9):091302, 2015.
- [15] E. Aprile et al. Search for Electronic Recoil Event Rate Modulation with 4 Years of XENON100 Data. 2017.
- [16] M Szydagis, A Fyhrie, D Thorngren, and M Tripathi. Enhancement of nest capabilities for simulating low-energy recoils in liquid xenon. *Journal of Instrumentation*, 8(10):C10003, 2013.
- [17] John Allison et al. Geant4 developments and applications. *IEEE Trans. Nucl. Sci.*, 53:270, 2006.
- [18] S. Agostinelli et al. GEANT4: A Simulation toolkit. *Nucl. Instrum. Meth.*, A506:250–303, 2003.
- [19] E Aprile et al. Observation and applications of single-electron charge signals in the xenon100 experiment. *Journal of Physics G: Nuclear and Particle Physics*, 41(3):035201, 2014.
- [20] E. Aprile, C. E. Dahl, L. DeViveiros, R. Gaitskell, K. L. Giboni, J. Kwong, P. Majewski, Kaixuan Ni, T. Shutt, and M. Yamashita. Simultaneous measurement of ionization and scintillation from nuclear recoils in liquid xenon as target for a dark matter experiment. *Phys. Rev. Lett.*, 97:081302, 2006.
- [21] E. Aprile et al. Dark Matter Results from 100 Live Days of XENON100 Data. *Phys. Rev. Lett.*, 107:131302, 2011.
- [22] E. Aprile et al. Response of the XENON100 Dark Matter Detector to Nuclear Recoils. *Phys. Rev.*, D88:012006, 2013.
- [23] Lorenzo Moneta, Kevin Belasco, Kyle S. Cranmer, S. Kreiss, Alfio Lazzaro, Danilo Piparo, Gregory Schott, Wouter Verkerke, and Matthias Wolf. The RooStats Project. *PoS, ACAT2010:057*, 2010.
- [24] Wouter Verkerke and David P. Kirkby. The RooFit toolkit for data modeling. *eConf*, C0303241:MOLT007, 2003. [186(2003)].
- [25] Glen Cowan, Kyle Cranmer, Eilam Gross, and Ofer Vitells. Asymptotic formulae for likelihood-based tests of new physics. *Eur. Phys. J.*, C71:1554, 2011. [Erratum: *Eur. Phys. J.* C73,2501(2013)].
- [26] Alexander L. Read. Modified frequentist analysis of search results (The CL(s) method). In *Workshop on confidence limits, CERN, Geneva, Switzerland, 17-18 Jan 2000: Proceedings*, pages 81–101, 2000.